ACS OMEGA

http://pubs.acs.org/journal/acsodf

Article

Method to Generate Random Element Equivalent Core Models Based on the NMR T_2 Spectrum for Waterflooding in Tight Sandstone

Rui Zhang and Hu Jia*

Cite This: *ACS Omega* 2021, 6, 34783−34795

Read Online

ACCESS | Metrics & More | Article Recommendations

ABSTRACT: Numerical simulation based on the widely used homogeneous equivalent core model can solve the problem of high cost and long duration of coreflooding experiments. However, using the homogeneous equivalent core model, it is difficult to reflect the characteristics of the core interior during waterflooding. In this paper, we provide a method to generate random element equivalent core models based on the nuclear magnetic resonance (NMR) T_2 spectrum, and it can divide permeability regions by granularity. The permeability calculation formula derived from the complementary correlation principle ensures that most areas of the core satisfy the correlation between permeability and T_2 relaxation time. Moreover, the generation method can guarantee that the random element equivalent core model is consistent with the homogeneous equivalent core model in terms of the geometric mean of permeability. The simulation results show that the high-resolution random element equivalent core model can better simulate microcosmic fingering inside the core during waterflooding. Nevertheless, the proposed method has some limitations emanating from the demarcation criteria and the porosity assumption. Furthermore, the generation method is expected to be extended to simulate enhanced oil recovery (EOR) mechanisms on the core scale after waterflooding.

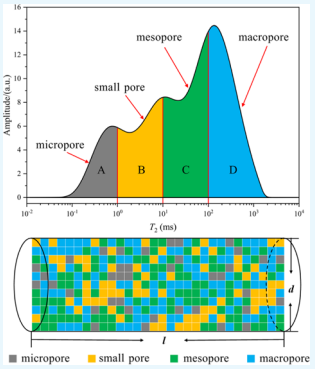

1. INTRODUCTION

Coreflooding experiment is an effective method to evaluate the oil displacement effect in petroleum engineering. It can be used to investigate the flow characteristics during the oil displacement process, which is of great significance to the design and optimization of enhanced oil recovery (EOR)[1] schemes. However, the high cost, long duration, and difficult measurement for coreflooding experiments are not conducive to the sensitivity analysis of parameters. Conversely, numerical simulation of the coreflooding experiment, as an experimental alternative, is an important method to obtain optimal parameters in the EOR process through a series of numerical tests. Generally, numerical simulation techniques can be classified as the pore scale, core scale, and reservoir scale. Reservoir scale numerical simulation can obtain the reservoir productivity characteristics and optimize the development plan.[2−4] Pore scale numerical simulation can reveal the microscopic seepage mechanism.[5−8] Currently, the research on coreflooding is mainly based on laboratory experiments. Moreover, a homogeneous equivalent core model is used to simulate the one-dimensional displacement process in most coreflooding numerical simulations.[9−13] In fact, core heterogeneity is of objective existence. Tight sandstones, as the representative unconventional reservoir, have low porosity and permeability, as well as complex pore structures, which affect the oil displacement characteristics of different areas in the core. Meanwhile, long duration and high pressure will greatly increase the difficulty of coreflooding experiments for tight sandstone. In addition, the homogeneous equivalent core model is difficult to fully characterize the oil displacement process because the conventional coreflooding experiments cannot detect the characteristics of the core interior. Therefore, it is of great significance to establish a new equivalent core model combined with core analysis technologies for high-resolution coreflooding numerical simulation.

Nuclear magnetic resonance (NMR) technology is widely used in the evaluation of reservoir pore structure in petroleum logging. As the relaxation mechanism of NMR is related to hydrogen atoms in the formation, it can provide pore and fluid information independent of the formation lithology.[14] Kleinberg et al.[15,16] investigated a series of NMR relaxation characteristics of fluids in cores, including the longitudinal relaxation time T_1, transverse relaxation time T_2, and the relationship between them. The NMR T_2 spectrum can be used to accurately calculate the total porosity of the reservoir.[17]

Received: September 25, 2021
Accepted: November 25, 2021
Published: December 8, 2021

Meantime, the pore structure of the complex reservoir can be continuously analyzed combined with the capillary pressure curve.[18,19] The response characteristics of the T_2 spectrum can also reflect the reservoir wettability[20−23] and fluid viscosity.[24,25] In addition, NMR technology has been extended to identify fluid properties.[26,27] With the development of NMR technology, it is possible to detect the change of oil and water content in coreflooding experiments by measuring the change of T_2 spectrum of the fluid in the core. Yang et al.[28] implemented NMR relaxometry measurements to determine residual oil distribution during waterflooding in tight oil formations. Liang et al.[29] used NMR technology to scan the coreflooding, which reflected the change of phase saturation and helped to understand the blocking mechanism of flow channels by gel rehydration. In recent years, many researchers have used the NMR T_2 relaxation distribution to study the migration of crude oil in pores during spontaneous imbibition,[30−34] indicating that NMR is a fast and non-destructive technique to reflect the hydrocarbon migration in tight porous media.

In this paper, the NMR T_2 spectrum is applied to the coreflooding numerical simulation in tight sandstones. The rest of this paper is organized as follows. Section 2 introduces the theory of NMR transverse relaxation time and the generation method of random element equivalent core model. Section 3 describes the coreflooding experiment including materials, experimental setup, experimental procedures, and history matching. Section 4 initiates result analysis and discussion. Some highlights are summarized in Section 5. The proposed method innovatively combines the NMR T_2 spectrum and core scale numerical simulation. Compared with the homogeneous equivalent core model, the method can better simulate microcosmic fingering inside the core during waterflooding, which provides a convenient visualization method for oil displacement characteristics during waterflooding in tight sandstone cores. Furthermore, the generation method is expected to be extended to simulate the EOR mechanisms on the core scale after waterflooding.

2. THEORY AND METHODOLOGY

2.1. NMR Transverse Relaxation Time. For fluids in porous media, there are three different relaxation mechanisms:

Table 1. Demarcation Criteria of Pore Region Class for Tight Sandstone Core Sample According to the NMR T_2 Spectrum

T_2	<1 ms	1−10 ms	10−100 ms	>100 ms
region class	A	B	C	D
pore type	micropore	small pore	mesopore	macropore

bulk relaxation, surface relaxation, and diffusion relaxation. As a result of these relaxation mechanisms, the NMR transverse relaxation time T_2 of a fluid in a pore can be expressed as follows[35]

$$\frac{1}{T_2} = \frac{1}{T_{2b}} + \frac{1}{T_{2s}} + \frac{1}{T_{2d}} \tag{1}$$

where T_{2b} is the transverse relaxation time of bulk fluid, T_{2s} is the surface relaxation time, and T_{2d} is the relaxation time as induced by diffusion. During the NMR measurement of the fluid in the core, T_{2b} and T_{2d} in eq 1 can usually be neglected.[36] Thus, T_2 is primarily dependent on T_{2s}, which is related to the specific surface area of a pore. Then, T_{2s} can be expressed by the following equation

$$\frac{1}{T_{2s}} = \rho\left(\frac{A}{V}\right)_{\text{pore}} \tag{2}$$

where ρ is the surface relaxivity, and A and V are the surface area and volume of the pore, respectively. $(A/V)_{\text{pore}}$, taken as a measure of the pore size, can be rewritten as a function of the pore radius r

$$\left(\frac{A}{V}\right)_{\text{pore}} = F_S/r \tag{3}$$

where F_S is the geometrical constant and its value depends on the pore shape. Inserting eq 3 into 2, we obtain

$$\frac{1}{T_{2s}} = \rho\frac{F_S}{r} \tag{4}$$

Assuming that ρ and F_s are constant for a core, the relationship between T_2 and r can be simplified to the following form[37]

$$T_2 = Cr \tag{5}$$

where C is a constant conversion coefficient between T_2 and r and $C = 1/(\rho F_s)$. After C is obtained, the NMR T_2 spectrum can be converted to a pore radius distribution.

2.2. T_2 Spectrum Division. According to eq 5, the NMR T_2 relaxation time can reflect the pore size, and the larger the T_2 relaxation time, the larger the pore radius. Liu et al.[38] and Zhou et al.[39] divided the pore types of sandstone into three types with the T_2 relaxation time boundary of 10 ms and 100 ms. As for tight sandstones, the pore types can be roughly divided into four classes according to the T_2 relaxation time, as shown in Table 1. The demarcation criteria are bounded by 1, 10, and 100 ms. As shown in Figure 1, the NMR T_2 spectrum can be divided into four regions according to the criteria. When a tight sandstone core sample is saturated with oil, each T_2 component of its T_2 spectrum is proportional to the porosity. Thus, region A, B, C, and D represent the percentage of micropore components, small pore components, mesopore components, and macropore components in the total porosity, respectively. It should be noted that saturated oil and water samples do not overlap in the relaxation time range. Therefore, the division of the T_2 distribution into sections is arbitrary and segmenting the T_2 spectrum is mainly to obtain the granularity required to build the random discrete model.

2.3. Permeability Calculation. The permeability of low porosity and permeability reservoirs is mainly affected by the rock pore structure. As a means to characterize the pore structure of the reservoir, NMR technology has obvious advantages in permeability evaluation. However, the Coates model and SDR model that are usually used to calculate permeability are mainly based on the macroscopic total volume ratio of connected pores in the rock.[40] Li et al.[41] analyzed the relationship between the permeability, porosity, and pore radius geometric mean by core analysis and found that permeability has a poor correlation with porosity, but has a very good correlation with the pore radius geometric mean. Thus, the relationship between permeability and pore radius can be expressed as follows

$$K_g = \alpha r_g \tag{6}$$

https://doi.org/10.1021/acsomega.1c05329
ACS Omega 2021, 6, 34783−34795

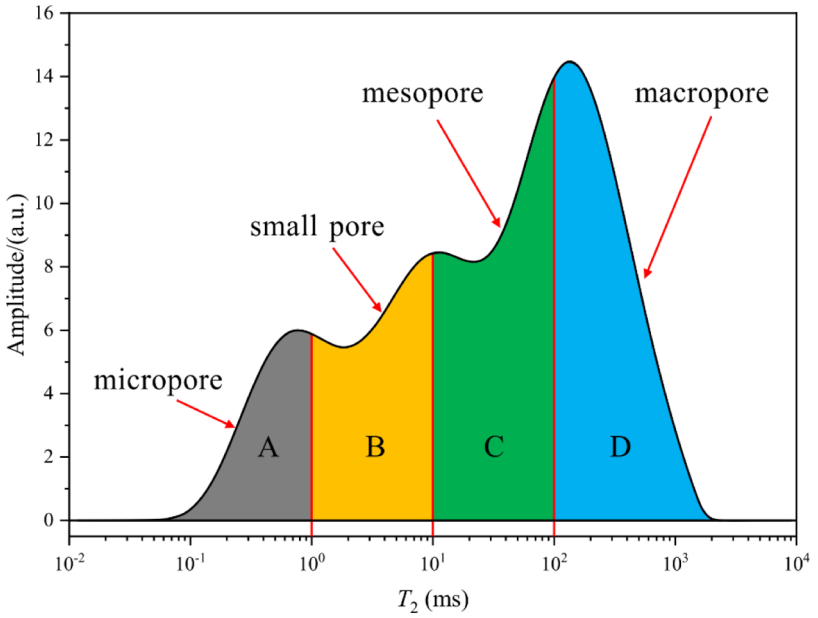

Figure 1. Diagram of region division according to the NMR T_2 spectrum.

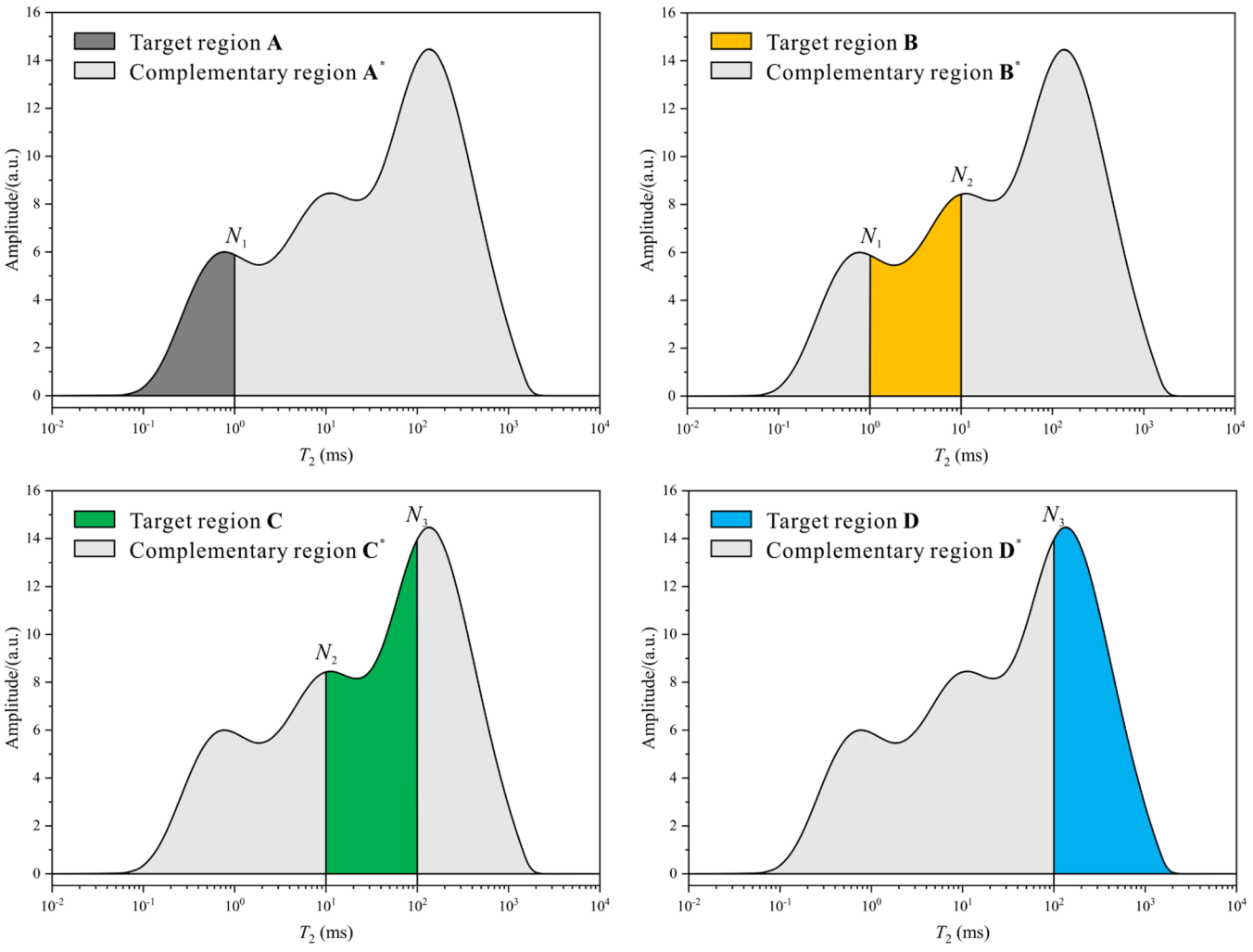

Figure 2. Diagram of permeability calculation in different regions according to the complementary correlation principle.

where K_g is the geometric mean of core permeability, which can be represented by the experimentally measured air permeability using the flowmeter method, r_g denotes the pore radius geometric mean, and α is the conversion coefficient

https://doi.org/10.1021/acsomega.1c05329
ACS Omega 2021, 6, 34783−34795

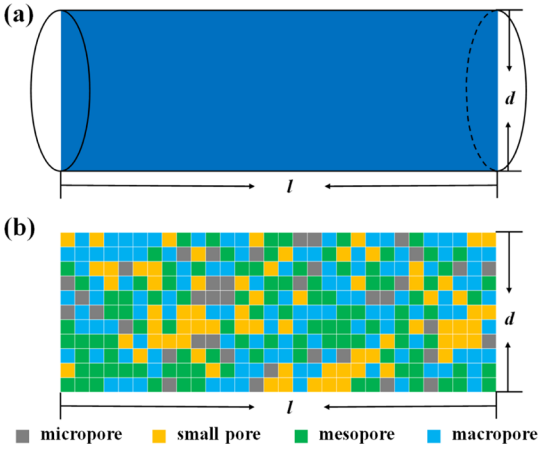

Figure 3. Diagram of the model generation. (a) Core axial section model. (b) Random element equivalent core model based on the NMR T_2 spectrum.

between K_g and r_g. Combining eqs 5 and 6 and defining the permeability conversion coefficient $C_g = \alpha/C$, we derive the relationship between permeability and T_2 relaxation time as follows

$$K_g = C_g T_{2g} \tag{7}$$

where T_{2g} is the geometric mean of the T_2 spectrum, which can be calculated by the following formula

$$T_{2g} = \left(\prod_{i=1}^{N} (T_{2i})^{M_i}\right)^{S} \tag{8}$$

where T_{2i} is the transverse relaxation time of the ith component, i = 1, 2, ..., N, M_i is the amplitude of the ith T_2 component, and S is the total amplitude of all T_2 components. The SDR model is also based on the geometric mean of T_2 spectrum, which can be expressed as follows[40]

$$K_g = C_g(\phi_{NMR})^m (T_{2g})^n \tag{9}$$

where ϕ_{NMR} is the total porosity measured by NMR, m and n are the uncertain parameters of the SDR model for which default values are 4 and 2, respectively. In the special case of m = 0 and n = 1, eq 9 can be transformed into eq 7. Compared with the SDR model, eq 7 ignores the influence of porosity on the permeability, which is conducive to the establishment of the random discrete model based on the assumption that all elements have the same porosity.

When the NMR T_2 spectrum of the tight sandstone core sample saturated with oil is obtained, T_{2g} can be calculated by eq 8. Then, C_g can be determined by eq 7 if the air permeability is measured. Figure 2 shows the diagram of permeability calculation in different regions according to the complementary correlation principle. The NMR T_2 spectrum is divided into two complementary parts of the target region (colored) and the complementary region (light gray). According to eq 7, the permeability of the complementary region can be calculated by the following formulas, which can ensure that most areas of the core satisfy the correlation as expressed in eq 7

$$\begin{cases} K_{c1} = C_g T_{2g1}, & K_{c2} = C_g T_{2g2} \\ K_{c3} = C_g T_{2g3}, & K_{c4} = C_g T_{2g4} \end{cases} \tag{10}$$

where K_{c1}, K_{c2}, K_{c3}, and K_{c4} represent the permeability of the complementary regions A*, B*, C*, and D*, respectively; T_{2g1}, T_{2g2}, T_{2g3}, and T_{2g4} represent the geometric mean of the T_2 spectrum in the complementary regions A*, B*, C*, and D* respectively, which can be calculated by the following formulas

$$\begin{cases} T_{2g1} = \left(\prod_{i=N_1}^{N} (T_{2i})^{M_i}\right)^{1/S_1}, \quad S_1 = \sum_{i=N_1}^{N} M_i \\ T_{2g2} = \left(\prod_{i=1}^{N_1} (T_{2i})^{M_i} \prod_{i=N_2}^{N} (T_{2i})^{M_i}\right)^{1/S_2}, \\ \quad S_2 = 1 - \sum_{i=N_1}^{N_2} M_i \\ T_{2g3} = \left(\prod_{i=1}^{N_2} (T_{2i})^{M_i} \prod_{i=N_3}^{N} (T_{2i})^{M_i}\right)^{1/S_3}, \\ \quad S_3 = 1 - \sum_{i=N_2}^{N_3} M_i \\ T_{2g4} = \left(\prod_{i=N_2}^{N} (T_{2i})^{M_i}\right)^{1/S_4}, \quad S_4 = \sum_{i=1}^{N_3} M_i \end{cases} \tag{11}$$

where S_1, S_2, S_3, and S_4 represent the total amplitude of all T_2 components in the complementary regions A*, B*, C*, and D*, respectively. According to the complementary relationship, the permeability calculation formulas in different target regions can be expressed as follows

$$\begin{cases} K_{t1} = \left(\dfrac{K_g}{(K_{c1})^{S_1/S}}\right)^{S/(1-S_1)}, \\ K_{t2} = \left(\dfrac{K_g}{(K_{c2})^{S_2/S}}\right)^{S/(1-S_2)} \\ K_{t3} = \left(\dfrac{K_g}{(K_{c3})^{S_3/S}}\right)^{S/(1-S_3)}, \\ K_{t4} = \left(\dfrac{K_g}{(K_{c4})^{S_4/S}}\right)^{S/(1-S_4)} \end{cases} \tag{12}$$

where K_{t1}, K_{t2}, K_{t3}, and K_{t4} represent the permeability of the target regions A, B, C, and D, respectively.

Overall, the permeability calculation based on the complementary correlation principle can be summarized as the following three steps: (1) to determine the permeability conversion coefficient by eq 7; (2) to obtain the permeability of the complementary region by eq 10; and (3) to calculate the permeability of the target region by eq 12.

2.4. Model Generation. As shown in Figure 3a, d and l denote the diameter and length of the core, respectively. To simplify the core model and reduce the simulation time, a core axial section model was created to analyze the dynamic characteristics and oil displacement effect during waterflooding in tight sandstones. In addition, the core axial section model has dimensions of d in the radial direction and l in the axial direction. According to the pore size, the core axial section

https://doi.org/10.1021/acsomega.1c05329
ACS Omega 2021, 6, 34783−34795

model can be divided into four types of elements, including the micropore, small pore, mesopore, and macropore. First, it is assumed that the porosity of each type of element is constant and equal to the total porosity of the core. Then, the proportion of each type of element in the core is computed according to the NMR T_2 spectrum. Next, the permeability parameters of different elements in the core are randomly assigned according to the proportion by MATLAB function: *randperm*. Finally, the random element equivalent core model based on the NMR T_2 spectrum is generated as shown in Figure 3b. It should be noted that the following relationship can be proved by eq 12

$$K_g = (K_{t1})^{(1-S_1)/S}(K_{t2})^{(1-S_2)/S}(K_{t3})^{(1-S_3)/S}(K_{t4})^{(1-S_4)/S} \quad (13)$$

Equation 13 indicates that the generation method can guarantee that the permeability geometric mean of the random element equivalent core model based on the NMR T_2 spectrum is equal to that of the homogeneous equivalent core model, which demonstrates the validity of the proposed method theoretically.

3. EXPERIMENTAL SECTION

3.1. Materials. In this study, a tight sandstone core sample was collected from Jilin oilfield for waterflooding and NMR experiments. The physical properties of the tight sandstone core sample are tabulated in Table 2. In order to differentiate the NMR signal of water from that of oil, a synthetic brine was prepared with deuterium oxide according to the brine salinity condition of a tight oil reservoir in Jilin oilfield. The density of the mineralized deuterium oxide (synthetic brine prepared with deuterium oxide) is 1.107 g/cm^3, and its viscosity is 1.25 mPa·s at 25 °C and atmospheric pressure. The simulated oil was prepared with Jilin tight oil and kerosene at a mass ratio of 1:2, and its density and viscosity are measured to be 0.828 g/cm^3 and 6.87 mPa·s, respectively, at 25 °C and atmospheric pressure.

Table 2. Physical Properties of the Tight Sandstone Core Sample

diameter (cm)	length (cm)	porosity (%)	permeability (mD)
2.48	6.27	9.69	2.44

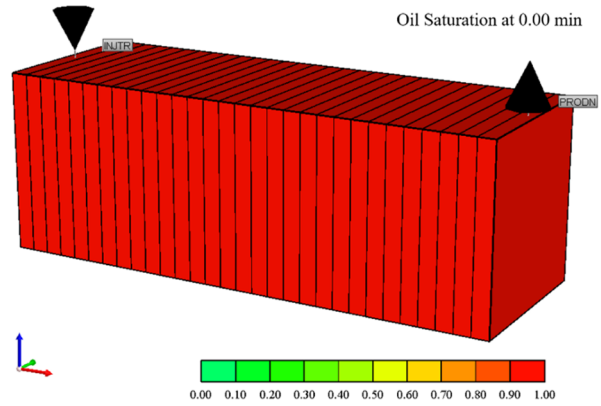

Figure 5. Three-dimensional homogeneous equivalent core model of the core sample showing the initial oil saturation.

3.2. Experimental Setup. As shown in Figure 4, the high temperature and high pressure coreflooding experimental setup is composed of an injection system, an analogue system, a measuring system, and an automatic control system. The injection system includes a high pressure syringe pump (ISCO, U.S.A.), one cylinder for storing the simulated oil and one cylinder for containing the mineralized deuterium oxide. The high pressure syringe pump is used to introduce simulated oil and mineralized deuterium oxide, respectively, to the tight core samples. The analogue system contains a core holder, a thermotank, an automatic pump, and a manual which are used to supply the confining pressure and return pressure for the core holder. The core holder has dimensions of 2.5 cm in diameter and 8.0 cm in length. The measuring system includes pressure measurement, temperature measurement, and flow measurement. Volume of the produced fluids is directly measured by reading the scale on the fluid sample collector, which is exposed under atmospheric pressure. The automatic control system can automatically control the flow of injection system, the automatic tracking of confining pressure, and the thermostat heating by a computer.

During the experiments, an NMR core analysis unit (SPEC-PMR-CTR, Beijing) is used to measure the NMR T_2 spectrum. The magnetic field strength of the NMR core analysis unit is 0.28 T and its resonance frequency for ^{1}H nuclei is 12 MHz. The maximum sample area has the dimensions of 3.0 cm in diameter and 4.0 cm in length, and a CPMG sequence is selected to measure the NMR T_2 spectrum. The spacing and

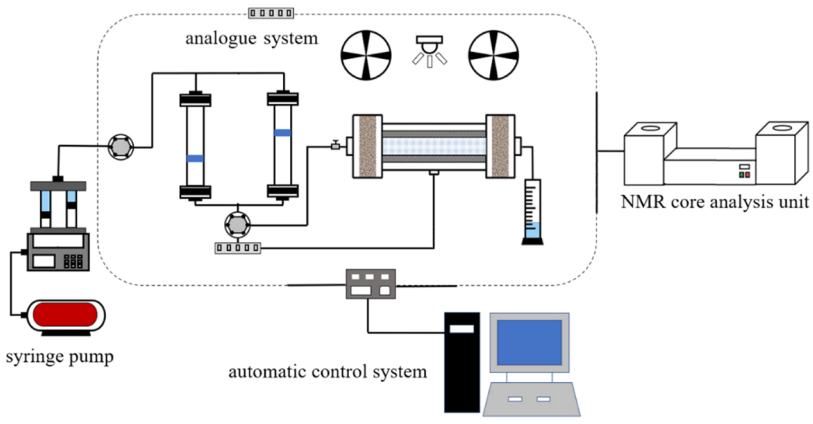

Figure 4. Schematic diagram of the coreflooding experimental setup.

https://doi.org/10.1021/acsomega.1c05329
ACS Omega 2021, 6, 34783−34795

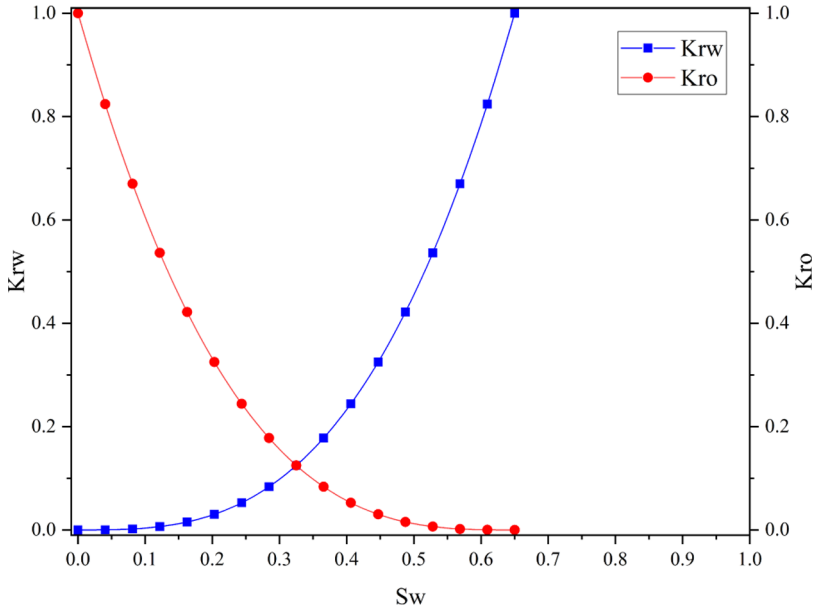

Figure 6. Relative permeability curves of the homogeneous equivalent core model.

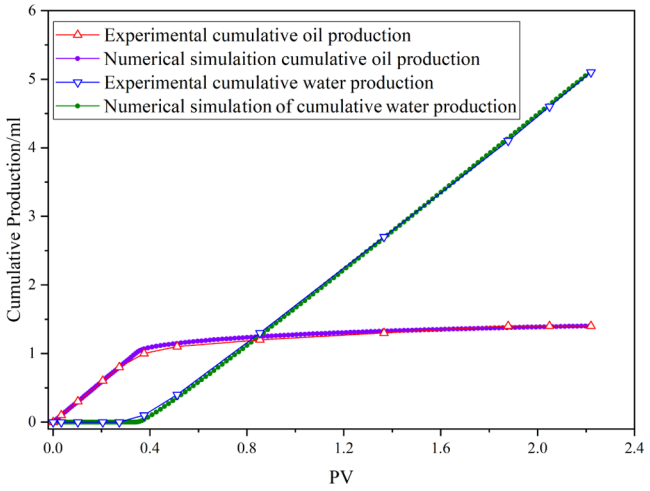

Figure 7. Fitting curves of cumulative production during waterflooding.

number of echo are 0.2 ms and 4096, respectively. The waiting and scan times are 3000 ms and 32, respectively.

3.3. Experimental Procedures. The experimental procedure used in this study is briefly described as follows. First, the tight sandstone core sample was dried in an oven at 90 °C for 24 h. After that, the diameter, length, and dry weight of the sample were measured. Then, the air permeability of the sample was measured by the flowmeter method. Second, a dry core was placed into the core holder to be vacuumized and to be displaced by injecting the simulated oil at 0.05 mL/min for 12 h. Then, the mass of saturated oil and the porosity of the core can be obtained by the weighting method. Third, the NMR T_2 spectrum of the oil-saturated core sample was measured using the NMR analysis unit. Fourth, the oil-saturated core sample was placed back into the core holder and displaced with mineralized deuterium oxide at 0.05 mL/min until the water cut of the produced fluids exceeds 98% or the oil volume of the produced fluids no longer increases. Finally, the NMR T_2 spectrum of the core sample flooding with mineralized deuterium oxide was measured using the NMR analysis unit. Besides, it should be noted that the confining pressure is automatically set to be 2−4 MPa higher than the inlet pressure of the core during all experiments. The coreflooding experiment was conducted at 90 °C and NMR off-line tests were carried out at a room temperature of 25 °C.

3.4. History Matching. As shown in Figure 5, a three-dimensional homogeneous equivalent core model was built using a commercial simulator CMG-IMEX,[42] with the direction of fluid flow being from the injector (INJTR) to producer (PRODN). The model was divided into 30 × 1 × 1 Cartesian grids, with each grid having a dimension of 0.2090 cm in I direction and 2.1978 cm in both J and K directions, thus the total volume of the model was equivalent to the bulk volume of the core sample. The model is homogeneous in porosity and permeability, the values of which are shown in Table 2. In addition, oil−water two-phase model was the selected model to characterize the fluids. Oil and water are assumed to be immiscible and incompressible. Fluid properties are set according to Section 3.1. Because the core is initially saturated with oil, the initial oil saturation of all grids is set to 1.0. The injector operates under a constant injection rate constraint of 0.05 mL/min, and the producer operates under a constant bottom-hole pressure constraint of an atmospheric pressure. The relative permeability of oil and water is adjusted to obtain a satisfactory match between the numerical simulation results and the experimental data on cumulative oil production and cumulative water production versus the fluid pore volume injected, and the relative permeability curves and the history matching results are shown in Figures 6 and 7, respectively. Apparently, the numerical simulation results and the experimental data on cumulative oil production and cumulative water production versus the fluid pore volume injected are well matched, which means that the obtained parameters can describe actual waterflooding in the porous media. Furthermore, these parameters can be used to study the dynamic characteristics and oil displacement effect during waterflooding in a random element equivalent core model based on the NMR T_2 spectrum as discussed in the next section.

https://doi.org/10.1021/acsomega.1c05329
ACS Omega 2021, 6, 34783−34795

4. RESULTS AND DISCUSSION

4.1. T_2 Spectra Analysis. Figure 8 shows the NMR T_2 spectra of original oil and residual oil in the tight sandstone core sample. The integral area of each curve represents the total volume of residual oil. We denote oil displacement efficiency as follows

$$E = (S_{ol} - S_{rl})/S_{ol} \quad (14)$$

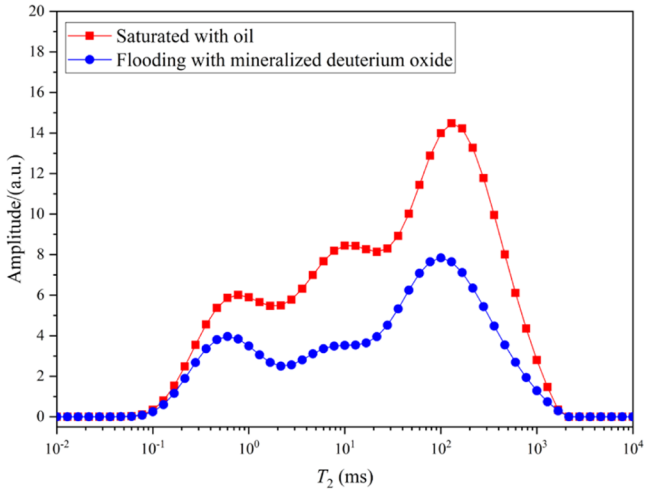

Figure 8. T_2 spectra of original oil and residual oil in the tight sandstone core sample.

Table 3. Region Oil Displacement Efficiency and Contribution of Oil Displacement Efficiency for Different Pore Regions

region class	A	B	C	D
region oil displacement efficiency/%	31	55	45	52
contribution of oil displacement efficiency/%	9	25	31	35

where E is the oil displacement efficiency based on T_2 spectra analysis; S_{ol} and S_{rl} are the total amplitude of all T_2 components for original oil and residual oil, respectively. It should be noted that the error of oil displacement efficiency based on T_2 spectra analysis mainly comes from two aspects. First, the signal-to-noise ratio of the NMR T_2 spectrum will affect the analysis accuracy of oil displacement efficiency and the signal-to-noise ratio is approximately 40 in this experiment. Second, it is better to clean excess oil at the core surface before conducting NMR analysis, which can improve the accuracy to some extent. From calculation, the oil displacement efficiency of mineralized deuterium oxide is 48%. Furthermore, according to the demarcation criteria of the pore region class in Table 1, the region oil displacement efficiency and contribution of oil displacement efficiency can be obtained. Table 3 shows the region oil displacement efficiency and contribution of oil displacement efficiency for different pore regions. It is apparent from this table that the region oil displacement efficiency and contribution of oil displacement efficiency for region A are 31 and 9%, respectively, which are significantly lower than other regions. It indicates that the micropore region is more difficult to be displaced by the injected water due to the relatively large resistance force. The experimental results show that the producing degree and oil displacement efficiency of different pore regions are different and it is of great significance to improve the oil displacement efficiency of the micropore region in tight sandstones. Regrettably, T_2 spectra can only qualitatively analyze the oil displacement efficiency of different pore regions. In the next section, a random element equivalent core model based on the NMR T_2 spectrum was used to visualize the dynamic characteristics inside the core sample during waterflooding.

4.2. Random Element Equivalent Core Model. As shown in Figure 9, four core axial section models including a homogeneous equivalent core model and three random element equivalent core models with different resolutions were constructed. The permeability and grid parameters of different equivalent core models are shown in Tables 4 and 5,

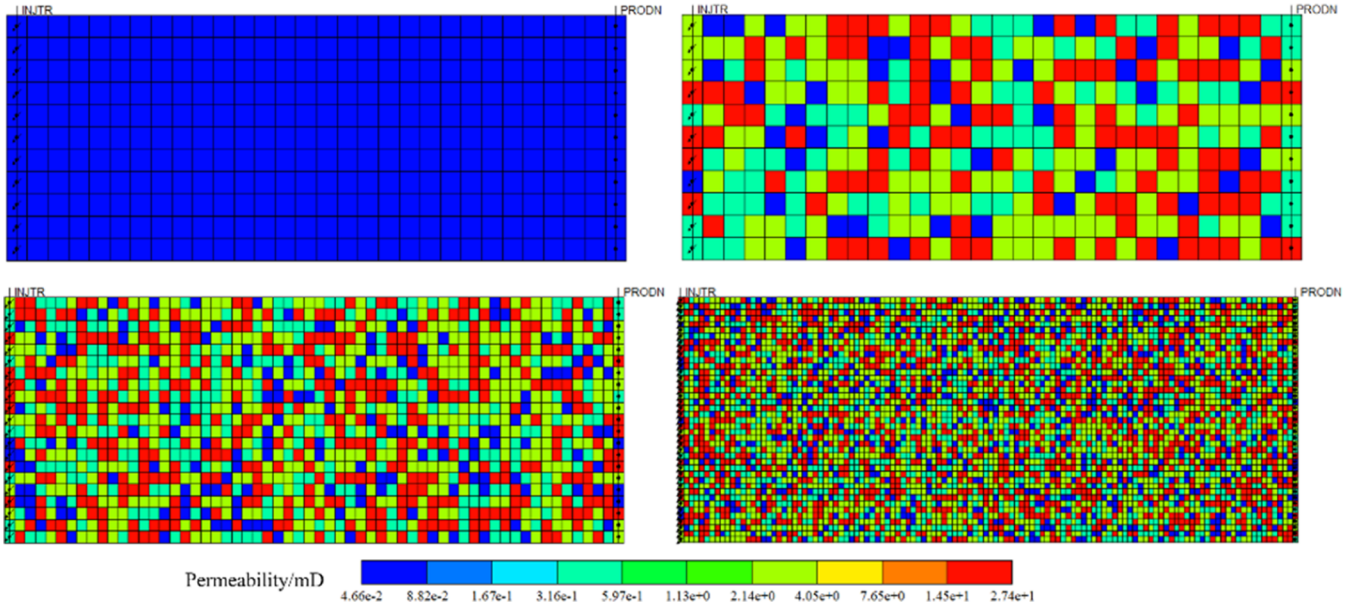

Figure 9. Four core axial section models including a homogeneous equivalent core model and three random element equivalent core models with different resolutions.

https://doi.org/10.1021/acsomega.1c05329
ACS Omega 2021, 6, 34783−34795

Table 4. Permeability Parameters of Different Equivalent Core Models

permeability parameters	region permeability/mD				permeability geometric mean/mD
	A	B	C	D	
homogeneous equivalent core model: 30 × 1 × 11	2.44				2.44
random element equivalent core model: 30 × 1 × 11	0.0466	0.3915	3.9927	27.4008	2.44
random element equivalent core model: 60 × 1 × 21	0.0466	0.3915	3.9927	27.4008	2.44
random element equivalent core model: 120 × 1 × 41	0.0466	0.3915	3.9927	27.4008	2.44

Table 5. Grid Parameters of Different Equivalent Core Models

grid parameters	grid dimension/cm			region grid number				total grid number
	I	*J*	*K*	A	B	C	D	
homogeneous equivalent core model: 30 × 1 × 11	0.2090	1.9478	0.2255	44	72	109	105	330
random element equivalent core model: 30 × 1 × 11	0.2090	1.9478	0.2255	44	72	109	105	330
random element equivalent core model: 60 × 1 × 21	0.1045	1.9478	0.1181	168	276	416	400	1260
random element equivalent core model: 120 × 1 × 41	0.0523	1.9478	0.0605	657	1079	1624	1560	4920

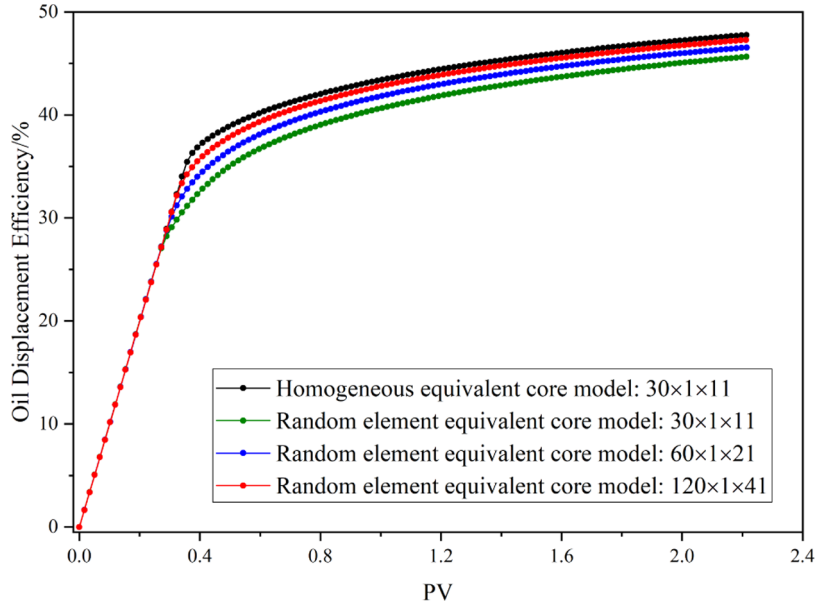

Figure 10. Oil displacement efficiency in the homogeneous equivalent core model and three random element equivalent core models with different resolutions.

respectively. The porosity of all grids in different equivalent core models is the same. The permeability of different pore regions in the random element equivalent core model was calculated by eq 12, and their geometric mean is equal to that of the homogeneous equivalent core model. It should be noted that the NMR T_2 spectrum used for model generation is obtained from an oil-saturated core sample, as shown by the red curve in Figure 8. Then, the model parameters of CMG-IMEX, including fluid properties, relative permeability curves and operations, are set according to the history matching in Section 3.4. Figure 10 shows the oil displacement efficiency in the homogeneous equivalent core model and three random element equivalent core models with different resolutions. It can be found that with the increase of resolution, the oil displacement efficiency of the random element equivalent core model is closer to that of the homogeneous equivalent core model. Figure 11 shows the oil saturation of the homogeneous equivalent core model at different times. It can be clearly seen that the oil saturation only changes in the displacement direction, which can only predict the water injection displacement front location inside the core and is difficult to fully characterize the oil displacement process. Figure 12 shows the oil saturation of two random element equivalent core models: 30 × 1 × 11 (left) and 120 × 1 × 4 (right) at different times. It can be seen intuitively in the figure that the injected water displaces the oil in the mesopore and macropore regions first because of the relatively small resistance force during waterflooding, which is also called fingering. Furthermore, the contrast analysis shows that the high-resolution random element equivalent core model can better simulate micro-cosmic fingering inside the core during waterflooding.

4.3. Injection Modes. The injection modes have an influence on the oil displacement effect of the core. Usually, there are two main injection modes of point injection and linear injection. According to the structural design of the core gripper plug section (Figure 13), some grooves will be added to the plug section to increase the contact area between the injected fluid and the core edge. As for the axial core section, three injection modes including linear injection, single-point injection, and multi-point injection, will occur in the axial section of the core when a plug with or without grooves is installed during waterflooding. Figure 14 shows oil saturation

https://doi.org/10.1021/acsomega.1c05329
ACS Omega 2021, 6, 34783−34795

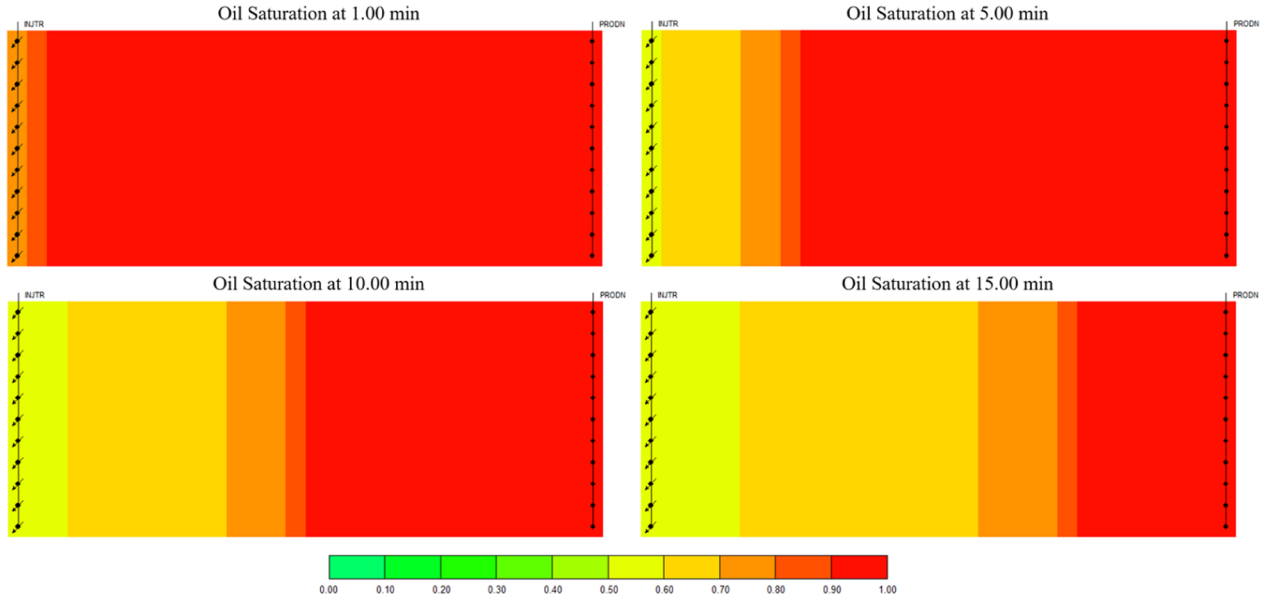

Figure 11. Oil saturation of the homogeneous equivalent core model at different times.

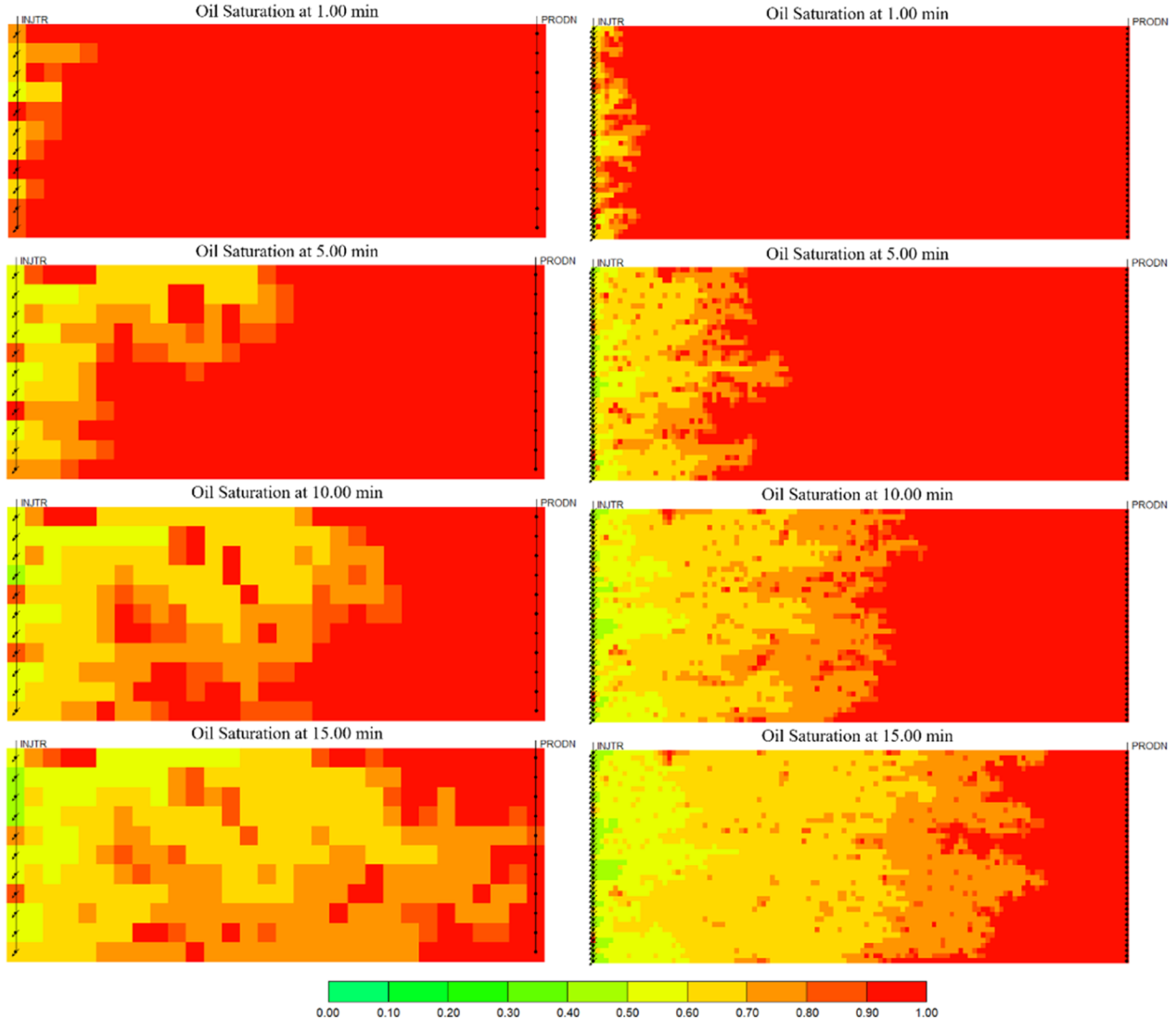

Figure 12. Oil saturation of two random element equivalent core models: 30 × 1 × 11 (left) and 120 × 1 × 41 (right) at different times.

https://doi.org/10.1021/acsomega.1c05329
ACS Omega 2021, 6, 34783−34795

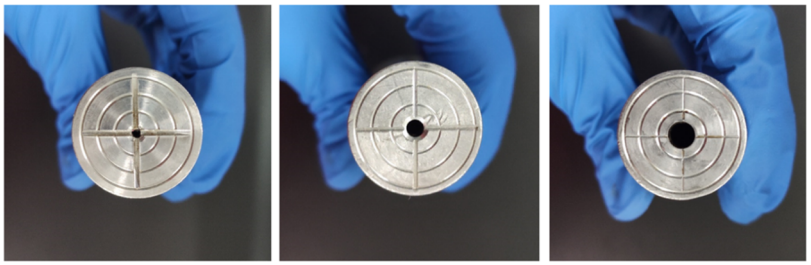

Figure 13. Structural design of the core gripper plug section.

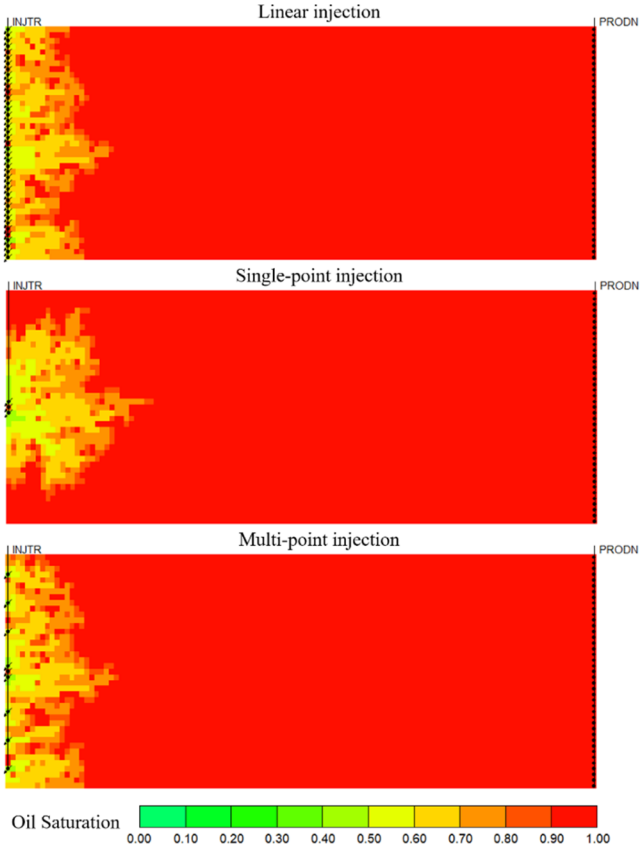

Figure 14. Oil saturation of the random element equivalent core model: 120 × 1 × 41 under different injection modes at 2 min.

of the random element equivalent core model: 120 × 1 × 41 under different injection modes at 2 min. Compared with linear injection, single-point injection does not sweep both sides of the core, whereas multi-point injection can achieve the sweeping effect of linear injection. Figure 15 shows the oil displacement efficiency and absolute error of the random element equivalent core model: 120 × 1 × 41 under different injection modes. There are differences in the oil displacement efficiency between single-point injection and linear injection, whereas there is no significant difference between multiple-point injection and linear injection. It shows that the difference of oil displacement efficiency of different axial sections inside the core can be reduced by adding grooves.

4.4. Permeability Random Distribution. In order to test the influence of permeability random distribution on the oil displacement efficiency, 10 cases for the random element equivalent core model: 120 × 1 × 41 were generated. Due to the random allocation of the MATLAB function: *randperm*, all cases have the same parameters except permeability distribution. Figure 16 shows the oil displacement efficiency and oil displacement efficiency variation of 10 cases. The average oil displacement efficiency of all cases is used as the benchmark to calculate the oil displacement efficiency variation. The oil displacement efficiency of different cases basically coincides with each other, and the oil displacement efficiency variation is less than 0.3%, indicating that the random distribution of permeability has little influence on the oil displacement efficiency. Therefore, when studying the influencing factors of oil displacement efficiency, the model generation method proposed in this paper can effectively avoid the interference of random permeability distribution on the oil displacement efficiency and is conducive to analyzing the influence of other factors.

5. CONCLUSIONS

In this paper, we propose an approach to generate a random element equivalent core model, where the permeability values used in the grid are based on the shape of the NMR T_2 distribution of a single-phase saturated rock sample, which is generally seen to reflect the pore size distribution within a rock. This random discrete model can be used to perform numerical flow simulations. The novel contribution of the work is to combine the NMR T_2 spectrum and core scale numerical simulation. The detailed conclusions can be drawn as follows.

- The permeability calculation formula derived from the complementary correlation principle ensures that most areas of the core satisfy the correlation between permeability and the T_2 relaxation time. Moreover, the generation method can guarantee that the random element equivalent core model is consistent with the homogeneous equivalent core model in terms of the geometric mean of permeability.
- With the increase of resolution, the oil displacement efficiency of the random element equivalent core model is closer to that of the homogeneous equivalent core model. Moreover, the high-resolution random element equivalent core model can better simulate microcosmic fingering inside the core during waterflooding.
- Numerical simulation results under different injection modes proved that the difference of displacement effect of different axial sections inside the core can be reduced by adding grooves. In addition, the sensitivity analysis result of random permeability distribution shows that the random distribution of permeability has little influence on the oil displacement efficiency, which is conducive to analyzing the influence of other factors.
- The two most important limitations of the proposed method are as follows. The division of the T_2 distribution into sections is arbitrary and segmenting the T_2 spectrum is mainly to obtain the granularity

https://doi.org/10.1021/acsomega.1c05329
ACS Omega 2021, 6, 34783−34795

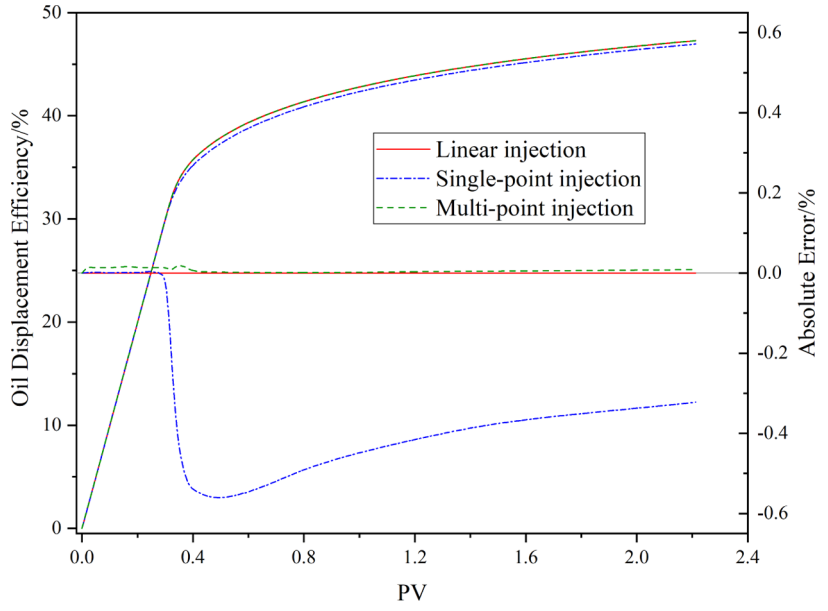

Figure 15. Oil displacement efficiency and absolute error of the random element equivalent core model: 120 × 1 × 41 under different injection modes.

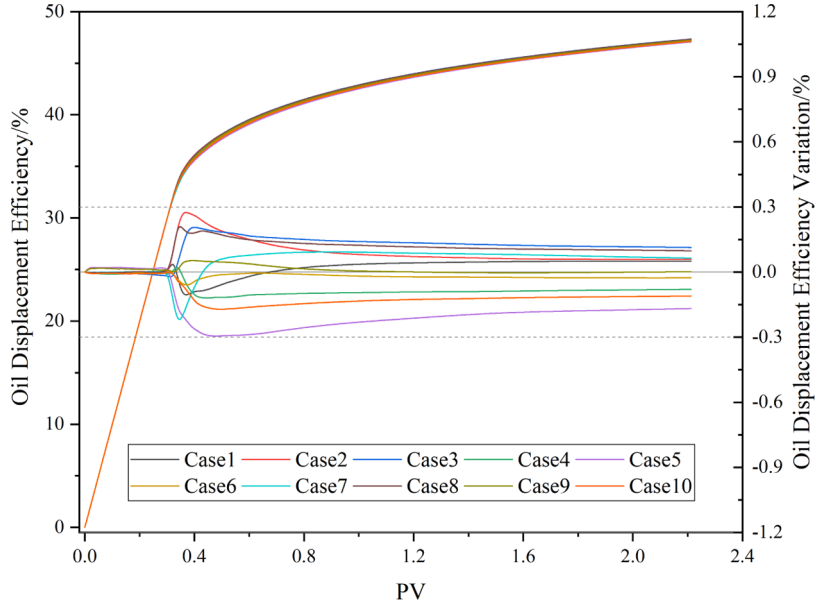

Figure 16. Oil displacement efficiency and oil displacement efficiency variation of 10 cases for the random element equivalent core model: 120 × 1 × 41.

required to build the random discrete model. The random discrete model is established based on the assumption that all elements have the same porosity; further work is needed to relax this assumption.

AUTHOR INFORMATION

Corresponding Author

Hu Jia − *State Key Laboratory of Oil and Gas Reservoir Geology and Exploitation, Southwest Petroleum University, Chengdu 610500, China;* orcid.org/0000-0001-9671-7791; Email: jiahuswpu@swpu.edu.cn

Author

Rui Zhang − *State Key Laboratory of Oil and Gas Reservoir Geology and Exploitation, Southwest Petroleum University, Chengdu 610500, China*

Complete contact information is available at: https://pubs.acs.org/10.1021/acsomega.1c05329

Notes

The authors declare no competing financial interest.

ACKNOWLEDGMENTS

This work was supported by Distinguished Young Scholars Fund in Sichuan (award no. 2019JDJQ0036), Fok Ying-Tong Education Foundation, China (grant no. 171043), and Youth

Science and Technology Innovation Team Fund of Southwest Petroleum University (award no. 2018CXTD08). We would like to thank the Computer Modeling Group Limited (CMGL), Calgary, Canada, for providing their reservoir simulators to Southwest Petroleum University.

NOMENCLATURE

T_2	transverse relaxation time, ms
T_{2b}	transverse relaxation time of bulk fluid, ms
T_{2s}	surface relaxation time, ms
T_{2d}	relaxation time as induced by diffusion, ms
ρ	surface relaxivity, μm/ms
A	surface area of the pore, μm^2
V	volume of the pore, μm^3
F_s	geometrical constant
r	pore radius, μm
C	constant conversion coefficient between T_2 and r, ms/μm
K_g	geometric mean of core permeability, mD
r_g	pore radius geometric mean, μm
α	conversion coefficient between K_g and r_g, mD/μm
C_g	permeability conversion coefficient, mD/ms
T_{2g}	geometric mean of the T_2 spectrum, ms
ϕ_{NMR}	total porosity measured by NMR
m	uncertain parameters of the SDR model
n	uncertain parameters of the SDR model
i	index of the component in the T_2 spectrum
N	number of the component in the T_2 spectrum
T_{2i}	transverse relaxation time of the ith T_2 component, ms
M_i	amplitude of the ith T_2 component
S	total amplitude of all T_2 components
K_{c1}	permeability of the complementary region A*, mD
K_{c2}	permeability of the complementary region B*, mD
K_{c3}	permeability of the complementary region C*, mD
K_{c4}	permeability of the complementary region D*, mD
T_{2g1}	geometric mean of the T_2 spectrum in the complementary region A*, ms
T_{2g2}	geometric mean of the T_2 spectrum in the complementary region B*, ms
T_{2g3}	geometric mean of the T_2 spectrum in the complementary region C*, ms
T_{2g4}	geometric mean of the T_2 spectrum in the complementary region D*, ms
S_1	total amplitude of all T_2 components in the complementary region A*
S_2	total amplitude of all T_2 components in the complementary region B*
S_3	total amplitude of all T_2 components in the complementary region C*
S_4	total amplitude of all T_2 components in the complementary region D*
K_{t1}	permeability of the target region A, mD
K_{t2}	permeability of the target region B, mD
K_{t3}	permeability of the target region C, mD
K_{t4}	permeability of the target region D, mD
d	diameter of the core, cm
l	length of the core, cm
E	oil displacement efficiency based on T_2 spectra analysis, %
S_{ol}	total amplitude of all T_2 components for original oil
S_{rl}	total amplitude of all T_2 components for residual oil

REFERENCES

(1) Lake, L. W. *Enhanced Oil Recovery*; Prentice Hall: Englewood Cliffs, 1989.
(2) Zhang, K.; Zhang, L.-m.; Yao, J.; Chen, Y.-x.; Lu, R.-r. Water flooding optimization with adjoint model under control constraints. *J. Hydrodyn. B* **2014**, *26*, 75−85.
(3) Zhang, K.; Zhang, H.; Zhang, L.; Li, P.; Zhang, X.; Yao, J. A new method for the construction and optimization of quadrangular adaptive well pattern. *Comput. Geosci.* **2017**, *21*, 499−518.
(4) Zhang, L.; Xu, C.; Zhang, K.; Yao, C.; Yang, Y.; Yao, J. Production optimization for alternated separate-layer water injection in complex fault reservoirs. *J. Pet. Sci. Eng.* **2020**, *193*, 107409.
(5) Raeini, A. Q.; Bijeljic, B.; Blunt, M. J. Numerical modelling of sub-pore scale events in two-phase flow through porous media. *Transp. Porous Media* **2014**, *101*, 191−213.
(6) Zhang, L.; Zhang, C.; Zhang, K.; Zhang, L.; Yao, J.; Sun, H.; Yang, Y. Pore-scale investigation of methane hydrate dissociation using the lattice Boltzmann method. *Water Resour. Res.* **2019**, *55*, 8422−8444.
(7) Liu, X.; Wang, L.; Wang, J.; Su, J. Pore-Scale Simulation of Particle Flooding for Enhancing Oil Recovery. *Energies* **2021**, *14*, 2305.
(8) Lin, W.; Xiong, S.; Liu, Y.; He, Y.; Chu, S.; Liu, S. Spontaneous imbibition in tight porous media with different wettability: Pore-scale simulation. *Phys. Fluids* **2021**, *33*, 032013.
(9) Kechut, N. I.; Jamiolahmady, M.; Sohrabi, M. Numerical simulation of experimental carbonated water injection (CWI) for improved oil recovery and CO_2 storage. *J. Pet. Sci. Eng.* **2011**, *77*, 111−120.
(10) Kuo, C.-W.; Benson, S. M. Analytical study of effects of flow rate, capillarity, and gravity on CO_2/brine multiphase-flow system in horizontal corefloods. *SPE J.* **2013**, *18*, 708−720.
(11) Feldmann, F.; Strobel, G. J.; Masalmeh, S. K.; AlSumaiti, A. M. An experimental and numerical study of low salinity effects on the oil recovery of carbonate rocks combining spontaneous imbibition, centrifuge method and coreflooding experiments. *J. Pet. Sci. Eng.* **2020**, *190*, 107045.
(12) Kumar, A.; Mandal, A. Core-scale modelling and numerical simulation of zwitterionic surfactant flooding: designing of chemical slug for enhanced oil recovery. *J. Pet. Sci. Eng.* **2020**, *192*, 107333.
(13) Wang, Y.; Liu, H.; Li, Y.; Wang, Q. Numerical Simulation of Spontaneous Imbibition under Different Boundary Conditions in Tight Reservoirs. *ACS Omega* **2021**, *6*, 21294−21303.
(14) Timur, A. Pulsed nuclear magnetic resonance studies of porosity, movable fluid, and permeability of sandstones. *J. Pet. Technol.* **1969**, *21*, 775−786.
(15) Kleinberg, R. L.; Straley, C.; Kenyon, W. E.; Akkurt, R.; Farooqui, S. A. Nuclear magnetic resonance of rocks: T_1 vs. T_2. *SPE Annual Technical Conference and Exhibition*, 1993.
(16) Kleinberg, R. L. Pore size distributions, pore coupling, and transverse relaxation spectra of porous rocks. *Magn. Reson. Imaging* **1994**, *12*, 271−274.
(17) Prammer, M. G.; Drack, E. D.; Bouton, J. C.; Gardner, J. S.; Coates, G. R.; Chandler, R. N.; Miller, M. N. Measurements of clay-bound water and total porosity by magnetic resonance logging. *SPE Annual Technical Conference and Exhibition*, 1996.
(18) Ausbrooks, R.; Hurley, N. F.; May, A.; Neese, D. G. Pore-size distributions in vuggy carbonates from core images, NMR, and capillary pressure. *SPE Annual Technical Conference and Exhibition*, 1999.
(19) Volokitin, Y.; Looyestijn, W. J.; Slijkerman, W. F.; Hofman, J. P. A practical approach to obtain primary drainage capillary pressure curves from NMR core and log data. *Petrophysics* **2001**, *42*, 334−343.
(20) Fleury, M.; Deflandre, F. Quantitative evaluation of porous media wettability using NMR relaxometry. *Magn. Reson. Imaging* **2003**, *21*, 385−387.
(21) Al-Mahrooqi, S. H.; Grattoni, C. A.; Muggeridge, A. H.; Jing, X. D. Wettability alteration during aging: The application of NMR to monitor fluid redistribution. *Society of Core Analyst*, 2005; pp 21−25.

https://doi.org/10.1021/acsomega.1c05329
ACS Omega 2021, 6, 34783−34795

(22) Looyestijn, W. J.; Hofman, J. Wettability-index determination by nuclear magnetic resonance. *SPE Reservoir Eval. Eng.* **2006**, *9*, 146−153.
(23) Shikhov, I.; Li, R.; Arns, C. H. Relaxation and relaxation exchange NMR to characterise asphaltene adsorption and wettability dynamics in siliceous systems. *Fuel* **2018**, *220*, 692−705.
(24) Bryan, J.; Kantzas, A.; Bellehumeur, C. Oil-viscosity predictions from low-field NMR measurements. *SPE Reservoir Eval. Eng.* **2005**, *8*, 44−52.
(25) Yang, Z.; Ma, Z.; Luo, Y.; Zhang, Y.; Guo, H.; Lin, W. A measured method for in situ viscosity of fluid in porous media by nuclear magnetic resonance. *Geofluids* **2018**, *2018*, 9542152.
(26) Hu, F.; Zhou, C.; Li, C.; Xu, H.; Zhou, F.; Si, Z. Water spectrum method of NMR logging for identifying fluids. *Pet. Explor. Dev.* **2016**, *43*, 268−276.
(27) Zhong, J.; Yan, R.; Zhang, H.; Feng, Y.; Li, N.; Liu, X. A decomposition method of nuclear magnetic resonance T_2 spectrum for identifying fluid properties. *Pet. Explor. Dev.* **2020**, *47*, 740−752.
(28) Yang, P.; Guo, H.; Yang, D. Determination of residual oil distribution during waterflooding in tight oil formations with NMR relaxometry measurements. *Energy Fuels* **2013**, *27*, 5750−5756.
(29) Liang, B.; Jiang, H.; Li, J.; Chen, F.; Miao, W.; Yang, H.; Qiao, Y.; Chen, W. Mechanism Study of Disproportionate Permeability Reduction Using Nuclear Magnetic Resonance T_2. *Energy Fuels* **2018**, *32*, 4959−4968.
(30) Wang, X.; Peng, X.; Zhang, S.; Du, Z.; Zeng, F. Characteristics of oil distributions in forced and spontaneous imbibition of tight oil reservoir. *Fuel* **2018**, *224*, 280−288.
(31) Cheng, Z.; Ning, Z.; Yu, X.; Wang, Q.; Zhang, W. New insights into spontaneous imbibition in tight oil sandstones with NMR. *J. Pet. Sci. Eng.* **2019**, *179*, 455−464.
(32) Yang, Z.; Liu, X.; Li, H.; Lei, Q.; Luo, Y.; Wang, X. Analysis on the influencing factors of imbibition and the effect evaluation of imbibition in tight reservoirs. *Pet. Explor. Dev.* **2019**, *46*, 779−785.
(33) Liu, J.; Sheng, J. J. Investigation of countercurrent imbibition in oil-wet tight cores using NMR technology. *SPE J.* **2020**, *25*, 2601−2614.
(34) Wang, C.; Gao, H.; Qi, Y.; Li, X.; Zhang, R.; Fan, H. Investigation on the Mechanisms of Spontaneous Imbibition at High Pressures for Tight Oil Recovery. *ACS Omega* **2020**, *5*, 12727−12734.
(35) Kleinberg, R. L.; Horsfield, M. A. Transverse relaxation processes in porous sedimentary rock. *J. Magn. Reson.* **1990**, *88*, 9−19.
(36) Gong, G.; Sun, B.; Liu, M.; Ye, C.; Gao, B. NMR relaxation of the fluid in rock porous media. *Chin. J. Magn. Reson.* **2006**, *23*, 379.
(37) Li, H.; Zhu, J.; Guo, H. Methods for calculating pore radius distribution in rock from NMR T2 spectra. *Chin. J. Magn. Reson.* **2008**, *25*, 273−280.
(38) Liu, Z.; Zhou, C.; Zhang, L.; Dai, D. J.; Li, C.; Zhang, L.; Shi, Y. An innovative method to evaluate formation pore structure using NMR logging data. *SPWLA 48th Annual Logging Symposium*, 2007.
(39) Zhou, C.; Liu, Z.; Zhang, L.; Dai, D.; Zhang, L.; Li, C.; Liu, G. Applications of NMR logs to complex lithology interpretation of ordos basin. *SPWLA 48th Annual Logging Symposium*, 2007.
(40) Coates, G. R.; Xiao, L.; Prammer, M. G. *NMR logging: principles and applications*; Haliburton Energy Services: Houston, 1999.
(41) Li, Z.; Cui, Y.; Guan, Y.; Wang, M. Permeability confirmation method of low porosity and permeability reservoirs based on pore distribution and T_2 spectrum. *J. China Univ. Pet., Ed. Nat. Sci.* **2018**, *42*, 34−40.
(42) CMG. *IMEX User's Guide*; Computer Modeling Group Ltd, 2015.

https://doi.org/10.1021/acsomega.1c05329
ACS Omega 2021, 6, 34783−34795